Surface symmetry energy of nuclear energy density functionals

N. Nikolov,[1,2] N. Schunck,[1,2,3] W. Nazarewicz,[1,2,4] M. Bender,[5] and J. Pei[1,2]

[1]*Department of Physics and Astronomy, University of Tennessee, Knoxville, Tennessee 37996, USA*
[2]*Physics Division, Oak Ridge National Laboratory, Oak Ridge, Tennessee 37831, USA*
[3]*Lawrence Livermore National Laboratory, P. O. Box 808, L-414 Livermore, California 94551, USA*
[4]*Institute of Theoretical Physics, University of Warsaw, ul. Hoża 69, PL-00-681 Warsaw, Poland*
[5]*Université Bordeaux I, CENBG/IN2P3, Centre d'Etudes Nucléaires de Bordeaux Gradignan, UMR5797,*
Chemin du Solarium, Boîte Postale 120, F-33175 Gradignan, France

We study the bulk deformation properties of the Skyrme nuclear energy density functionals (EDFs). Following simple arguments based on the leptodermous expansion and liquid drop model, we apply the nuclear density functional theory to assess the role of the surface symmetry energy in nuclei. To this end, we validate the commonly used functional parametrizations against the data on excitation energies of superdeformed band heads in Hg and Pb isotopes and fission isomers in actinide nuclei. After subtracting shell effects, the results of our self-consistent calculations are consistent with macroscopic arguments and indicate that experimental data on strongly deformed configurations in neutron-rich nuclei are essential for optimizing future nuclear EDFs. The resulting survey provides a useful benchmark for further theoretical improvements. Unlike in nuclei close to the stability valley, whose macroscopic deformability hangs on the balance of surface and Coulomb terms, the deformability of neutron-rich nuclei strongly depends on the surface symmetry energy; hence, its proper determination is crucial for the stability of deformed phases of the neutron-rich matter and description of fission rates for r-process nucleosynthesis.

I. INTRODUCTION

Ongoing efforts to develop the nuclear energy density functional (EDF) of spectroscopic quality are faced with the challenge to find optimal experimental and theoretical constraints that would help us pin down its various coupling constants. Traditional parametrizations of nuclear EDFs, such as Skyrme and Gogny often rely, through the fitting protocol applied, on a combination of carefully selected experimental data as well as pseudodata characterizing properties of nuclear matter (see, e.g., the discussions in Refs. [1–5]). Considering the fairly simple forms (and small number of coupling constants) of commonly used nuclear EDFs, the success of the nuclear density functional theory (DFT) to describe a wide range of nuclear properties has been truly remarkable. However, the robustness of these parametrizations when going away from the neighborhood of the stability valley, where experimental data are abundant, to the neutron-rich region where data are scarce or nonexistent, is questionable. Indeed, large differences in predictions for very neutron-rich or superheavy elements seen for various EDFs [6–8] is highly unsatisfactory. In fact, recent systematic studies of Skyrme EDFs showed that some coupling constants cannot be properly constrained by existing data and that the current forms of EDFs are too limiting [9,10]. Moreover, early attempts to employ statistical methods of linear regression and error analysis [11] have been revived recently and have been applied to determine the uncertainties of EDF parameters, errors of calculated observables, and to assess the quality of theoretical extrapolations [4,10,12–14]. The major uncertainty in nuclear EDFs lies in the isovector channels that are poorly constrained by experiment; hence, new data on unstable nuclei with large

neutron excess that have a large lever arm from the valley of stability are essential [15].

The pool of fit observables entering the optimization protocol of EDFs, usually contains experimental data characterizing both bulk (global) and local nuclear properties, as well as theoretical pseudodata pertaining to global nuclear matter properties (NMPs). The characterization in terms of bulk and local nuclear properties is not very precise and somehow arbitrary; it has its origin in the macroscopic-microscopic approach, which offers a description in terms of a macroscopic liquid drop (LD) (whose properties change smoothly as a function of nucleon numbers) and shell correction that oscillates rapidly with shell filling [16–19]. In the context of DFT, the binding energy of a nucleus of mass A and neutron excess $I = (N - Z)/A$ can be split into a smooth function of I and A, and a fluctuating shell correction term by means of the Strutinsky energy theorem [16,20–23]. This theorem, together with the shell-correction method, offers a formal framework to link the self-consistent DFT with macroscopic-microscopic models that often provide useful insights in terms of the liquid drop (or droplet) model (LDM) and shell effects.

Single-particle shell structure can be accessed through, for example, experimental separation energies and single-particle strength. Such fit observables are often used in the determination of EDF parametrizations [1,24]. Similarly, the volume and symmetry terms of the LDM [25,26] are related to nuclear matter properties, which are relatively well determined. This effectively constrains specific combinations of parameters of the EDF. However, surface terms of the LDM are harder to pin down. In a recent work [27], the leptodermous expansion of the nuclear binding energy was revisited, and the LDM parameters of several EDFs were extracted from

DFT calculations for very large nuclei. While the surface and curvature terms came out to be fairly robust, it was found that the surface symmetry coefficient a_{ssym} of the LDM could vary by a factor of 3 across the set of parametrizations. This coefficient enters the expression for the symmetry energy in the spherical LDM,

$$\frac{E_{\mathrm{sym}}^{\mathrm{LDM}}}{A} = \left(a_{\mathrm{sym}} + \frac{a_{\mathrm{ssym}}}{A^{1/3}} \right) I^2, \tag{1}$$

where a_{sym} is the (volume) symmetry energy coefficient. A thorough compilation of symmetry energy coefficients obtained in different EDFs, assuming various definitions, can be found in Sec. 4.7 of Ref. [28].

In early Hartree-Fock (HF) and extended-Thomas-Fermi studies [29–32] using various EDFs, a correlation between a_{ssym} and a_{sym} was pointed out. Namely, EDFs having large values of a_{sym} also have large $|a_{\mathrm{ssym}}|$. Since the surface symmetry coefficient is negative, these two terms act in opposite directions in E_{sym}. The correlation between bulk and surface symmetry energies was further discussed in Refs. [28,33–36]; it was concluded that the presence of the correlation makes an absolute determination of a_{sym} and a_{ssym} from nuclear masses difficult (see also discussion in an early Ref. [37]).

The experimental information about a_{ssym} is fairly limited. The ratio of the surface symmetry to symmetry (or volume symmetry) coefficients, $r_{S/V} = a_{\mathrm{ssym}}/a_{\mathrm{sym}}$, has been estimated from the electric dipole strength distribution [38], masses [36,39–41], masses and radii [33,35], and excitation energies of isobaric analog states [42]. Recently, an attempt has been made to extract a_{ssym} [43] from the separation energies through the displacement of neutron and proton chemical potentials. They noted a large A variation of $r_{S/V}$. As discussed later, the DFT values of $r_{S/V}$ obtained in Refs. [27,28,44] are fairly consistent with phenomenological estimates.

Since the absolute value of a_{ssym} is not well constrained by experimental data on ground-state (g.s.) nuclear properties, one needs to find some mechanism that would enhance the surface symmetry term with respect to the dominant volume symmetry energy. Since the surface symmetry energy increases with both neutron excess and nuclear surface area, it is anticipated that strongly deformed configurations of nuclei with appreciable neutron excess can be of help. Indeed, the nuclear shape deformation increases the surface area, thus, amplifying the surface symmetry energy in a neutron-rich nucleus. Conversely, the precise determination of surface symmetry energy is important to describe the deformability of neutron-rich systems and to validate theoretical extrapolations. In this context, one can mention several phenomena involving neutron excess and deformation:

(i) *Position of the neutron drip line*. Deformed nuclei are expected in several regions near the neutron drip line [45,46]. In some cases, deformation energy can impact their mere existence. For instance, it has been predicted that there exist particle-bound even-even nuclei that have, at the same time, negative two-neutron separation energies caused by shape coexistence effects [45].

(ii) *Borders of the superheavy region*. The super- and hyperheavy nuclei with $Z > 126$ can exist in states associated with very exotic topologies of nuclear density as the competition between Coulomb, surface, symmetry, and shell effects can give rise to formation of voids [47]. The subject of exotic (bubble, toroidal, and bandlike) configurations in nuclei with very large atomic numbers has been addressed by several studies [48–51]. At present, it is difficult to say whether these exotic topologies can occur as metastable states [50] and what is their stability to various shape deformations.

(iii) *Fusion and fission of neutron-rich nuclei*. Synthesis of heavy and superheavy neutron-rich nuclei is profoundly affected by nuclear deformability through the energetics of fusion and fission valleys [52,53]. Our ability to describe fission of neutron-rich systems is also important for modeling nuclear reactors. While DFT calculations are currently able to predict barrier heights of known nuclei with a typical accuracy of 20%, the resulting uncertainties in fission cross sections are still large [46]. The ability of modern nuclear EDFs to predict neutron-induced fission rates for neutron-rich nuclei that cannot be measured is crucial. At this point, the dependence of rates on fission barriers is appreciable [54].

(iv) *Rotational properties of neutron-rich nuclei*. Nuclear deformation determines the response of the nucleus to angular momentum. Little is known about the collective rotation of very neutron-rich systems [55] and the corresponding interplay between deformation–isospin, and rotation.

(v) *Astrophysical r process*. Fission of neutron-rich nuclei impacts the formation of heavy elements at the final stages of the r process through the recycling mechanism [56,57]. The fission recycling is believed to be of particular importance during neutron star mergers where free neutrons of high density are available [54,57]. Also, neutrino-induced fission of neutron-rich nuclei could affect the r-process flow in some scenarios [58].

(vi) *Structure of neutron stars*. Nucleonic phases in the inner crust of neutron stars are associated with very neutron-rich deformed nuclei or strongly deformed pasta and antipasta phases [59,60].

The primary motivation of this paper is to assess the role played by the surface symmetry energy in neutron-rich nuclei. To this end, we study the surface symmetry contribution to the LDM energy and demonstrate that it may be as important as the Coulomb term in driving deformation properties of very neutron-rich systems. Using the self-consistent DFT, we survey excitation energies of superdeformed (SD) states in the Hg-Pb region and SD fission isomers in the actinides. By subtracting microscopic shell corrections, we extract the macroscopic part of the HF deformation energy and demonstrate that the outcome is consistent with qualitative macroscopic estimates. Our results indicate that experimental data on strongly deformed configurations in neutron-rich nuclei are key for optimizing the isospin channel of the nuclear EDF.

Our paper is organized as follows. In Sec. II, based on the spherical and deformed LDM, we discuss general properties of the surface symmetry term. In particular, we analyze symmetry energy parameters of various Skyrme EDFs, study global correlations between a_{ssym} and a_{sym}, and show how to disentangle the surface symmetry term by studying deformed configurations in nuclei with nonzero neutron excess. Self-consistent DFT calculations of fission isomers in the actinides and band heads of SD rotational bands in the $A \sim 190$ region are presented in Sec. III. The methodology used to extract the smooth contribution to the total energy is outlined in Sec. IV. Section V presents our calculations of the smooth contributions to the deformation energy of SD states and compares Hartree-Fock-Bogoliubov (HFB) and LDM results. Finally, the conclusions of our work are given in Sec. VI.

II. LDM FROM THE SKYRME EDF

The LDM provides a convenient parametrization of the bulk part of the binding energy of a spherical even-even nucleus with Z protons and N neutrons. Expressed in terms of volume (a_{vol}), surface (a_{surf}), curvature (a_{curv}), symmetry, surface symmetry, Coulomb, and Coulomb exchange parameters, it reads

$$
\begin{aligned}
E_{\text{sph}}^{\text{LDM}} = {} & a_{\text{vol}}A + a_{\text{surf}}A^{2/3} + a_{\text{curv}}A^{1/3} \\
& + a_{\text{sym}}I^2 A + a_{\text{ssym}}I^2 A^{2/3} + a_{\text{sym}}^{(2)}I^4 A \\
& + \frac{3}{5}\frac{e^2}{r_0^{\text{ch}}}\frac{Z^2}{A^{1/3}} - \frac{5}{4}\left(\frac{3}{2\pi}\right)^{2/3}\frac{3}{5}\frac{e^2}{r_0^{\text{ch}}}\frac{Z^{4/3}}{A^{1/3}},
\end{aligned} \quad (2)
$$

where e is the electric charge and r_0^{ch} is the Wigner-Seitz radius. The justification of Eq. (2) can be given in terms of the leptodermous expansion valid for systems with a well-developed surface [61–63] that sorts the various contributions to the binding energy of finite nuclei in terms that have transparent physical meaning. The expansion (2) can be extended to higher orders [64,65]. The second-order symmetry energy term $\propto I^4$ is not always included in the macroscopic LDM, but it is naturally present in the microscopic LDM expression [27].

A. Approaches to bulk nuclear properties

Some LDM parameters are fundamental NMPs and can be determined microscopically from *ab initio* calculations of the equation of state of nucleonic matter [66–68]. Another phenomenological strategy is to obtain LDM constants, or at least some of them, from a direct fit to selected experimental data from finite nuclei. The original work of Myers and Swiatecki followed such a strategy [69]: By modeling local fluctuations in particle numbers caused by shell effects, one can extract smooth LDM trends from experimental nuclear masses. Subsequent refinements involved the upgrade from a simple drop to a more accurate droplet model [26], which allowed pinning down additional terms in the leptodermous expansion. Further refinements can be found in, for example, Refs. [39,64,70–72].

Just as in the microscopic approach, whose outcome depends on both the input (i.e., nucleon-nucleon interactions) and the theoretical method used to solve the many-body problem, the results of phenomenological procedure depend on the choice of fit observables and prescription used to compute shell corrections (see Ref. [73] for a recent concise overview of this topic). There are significant correlations among the different LDM terms, and some parameters are poorly determined [36]. In particular, precise extraction of higher-order isospin-dependent terms requires abundant data for very neutron-rich and/or heavy nuclei, which are not available at present.

B. Spherical LD based on DFT

An advantage of the macroscopic approach to bulk nuclear properties is that it can also be applied in the context of the nuclear DFT. While some LDM constants pertaining to infinite or semi-infinite NMP can be extracted from EDF parametrizations [1,28,74], surface and curvature terms are best determined by using the semiclassical approach [75,76] or by removing the contribution from shell effects from self-consistent DFT results [23]. There are relatively few examples of latter studies in the literature, and most were confined to spherical symmetry. In Ref. [77], the parameters a_{vol}, a_{sym}, a_{surf}, a_{ssym}, and r_0^{ch} were estimated from spherical HFB calculations using the finite-range Gogny force D1S [78]. In Ref. [79], a similar work was carried out for the NL3 parametrization of the relativistic mean field (RMF) [80].

This program was carried out more systematically in Ref. [27] for Skyrme EDFs and several parametrizations of RMF Lagrangians using the HF method. The main difference with Refs. [77,79] is that the convergence of the leptodermous expansion was tested using an extended sample of very large spherical nuclei. The Coulomb terms were ignored to be able to approach nuclei of arbitrary sizes and to avoid radial instabilities (Coulomb frustration) characteristic of systems with many protons. The shell corrections were extracted from the HF results according to Green's function method and the generalized Strutinsky smoothing procedure of Refs. [81–83]. Table I displays the values of the symmetry, surface symmetry, and surface coefficients for various realizations of the nuclear EDF. These values are fairly close to those obtained in Ref. [28]. We also note that, in the case of NL3, there are relatively large differences between the values in Table I and those reported in Ref. [79]: These can be attributed to different ways of extracting the shell correction and fitting the LD formula (sample size, treatment of the Coulomb term).

As noted in Ref. [27], the leading surface and symmetry terms appear relatively similar within each family of EDFs, with a clear difference for a_{sym} between nonrelativistic and relativistic approaches. Obviously, even small variations in a_{surf} and a_{sym} seen in Table I can have an appreciable impact on the binding energy, as these coefficients are multiplied by large A- and I^2-dependent factors [27]. For the surface symmetry coefficient, however, there are much larger discrepancies. For Skyrme EDFs, for instance, there is a factor of 2 between the largest and smallest values. This demonstrates that a_{ssym} is

TABLE I. Surface, symmetry, and surface symmetry LDM coefficients (in MeV) of various EDFs extracted from leptodermous expansion in Ref. [27]. The Skyrme EDF parametrizations are SkM* [84], SkP [85], BSk1 [86], BSk6 [87], SLy4-SLy6 [88], SkI3-SkI4 [89], and SkO [90]. The RMF Lagrangians are NL1 [91], NL-Z [92], and NL-Z2 [93]. For comparison, the results of LDM fits are given as LDM$^{(1)}$ [39] and LDM$^{(2)}$-LSD [72].

EDF	a_{surf}	a_{sym}	a_{ssym}	EDF	a_{surf}	a_{sym}	a_{ssym}
SkM*	17.6	30.04	−52	NL1	18.8	43.48	−110
SkP	18.2	30.01	−45	NL3	18.6	37.40	−86
BSk1	17.5	27.81	−36	NL-Z	17.8	41.74	−125
BSk6	17.3	28.00	−33	NL-Z2	17.4	39.03	−90
SLy4	18.4	32.01	−54				
SLy6	17.7	31.96	−51	LDM$^{(1)}$	21.1	30.56	−48.6
SkI3	18.0	34.84	−75	LDM$^{(2)}$	19.4	29.28	−38.4
SkI4	17.7	29.51	−34	LSD	17.0	28.82	−38.9
SkO	17.3	31.98	−58				

very poorly constrained in the current EDF parametrizations (see also the discussion in Ref. [28]).

In addition, as discussed in Sec. I, there appears a clear (anti)correlation between the (positive) value of the symmetry coefficient and the (negative) value of the surface symmetry coefficient [28–36]. Figure 1, displays the pairs $(a_{\mathrm{ssym}}, a_{\mathrm{sym}})$ for the Skyrme EDFs of Table I and the EDFs of Ref. [28]. The ratio $r_{S/V}$ extracted from experimental masses is $r_{S/V} \approx -1.7$ [36]. When looking into details, however, it exhibits a large A variation [43]; $r_{S/V}$ ranges between -1 (for $A \geqslant 12$) and -1.7 (for $A \geqslant 50$). As discussed in Ref. [44], the data on the electric dipole polarizability yield $r_{S/V} \approx -1.65$. The DFT values shown in Fig. 1 are not inconsistent with these phenomenological estimates. While a correlation between a_{sym}
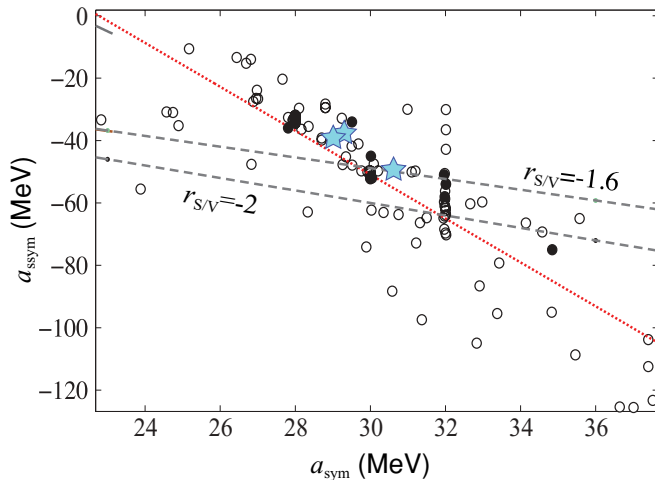

FIG. 1. (Color online) Correlation between the symmetry and surface symmetry coefficients extracted from Skyrme EDFs from Table I (dots) and Skyrme EDFs of Ref. [28] (circles). The phenomenological LDM values of Table I are also indicated (stars) as well as the hydrodynamical [38] and mass [43,44] estimates: $r_{S/V} = -2$ and -1.6, respectively (dashed lines). The linear fit to the values of Ref. [28] is shown by a dotted line.
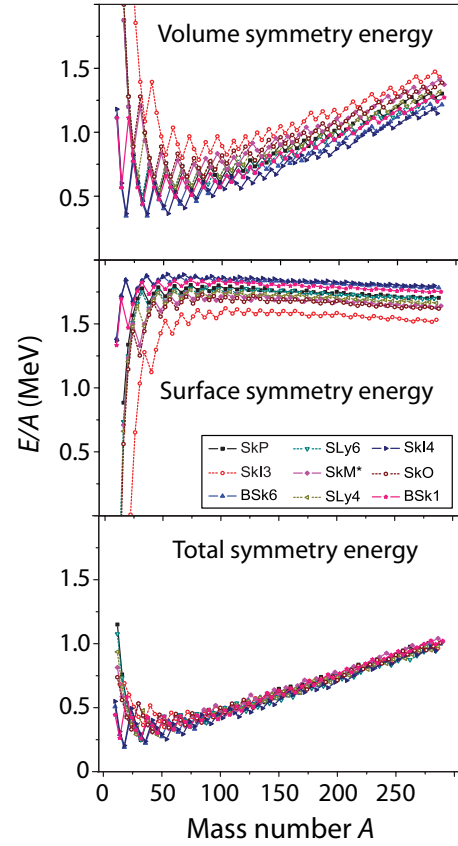

FIG. 2. (Color online) Contributions to the microscopic LDM energy per nucleon along the LDM valley of stability: volume symmetry term $a_{\mathrm{sym}} I^2$ (top), surface symmetry term $a_{\mathrm{ssym}} I^2 A^{-1/3}$ (middle), and the total symmetry energy (bottom) for the microscopic LDM derived from Skyrme EDFs of Table I.

and a_{ssym} is clear, a very large spread of values is indicative of the inability of current data on g.s. nuclear properties to adequately constrain a_{ssym}. It is interesting to note that the LDM values of Table I and phenomenological estimates cluster around $a_{\mathrm{sym}} = 30$ MeV and $a_{\mathrm{ssym}} = -45$ MeV.

To get more insight into the consequences of this observation, in Fig. 2, we plot the symmetry and surface symmetry contributions to the binding energy per nucleon E^{LDM}/A for the microscopic LDM derived from Skyrme EDFs listed in Table I along the LDM valley of stability. The latter one is defined by minimizing the LDM energy in the (Z, N) plane. The symmetry energy slightly increases with mass number (upper panel), owing to the fact that the valley of stability bends down for increasing Z so that the energy per nucleon $E_{\mathrm{sym}} = a_{\mathrm{sym}} I^2$ increases. Contrariwise, the surface symmetry energy slightly decreases with A because of the $A^{-1/3}$ dependence.

Interestingly, the total symmetry energy (i.e., the sum of volume and surface contributions) exhibits much smaller spread between various EDFs: from about $0.4/A$ MeV for both E_{sym}/A and E_{ssym}/A to about $0.1/A$ MeV for the sum. This is a consequence of the aforementioned correlation between volume and surface symmetry energies that implies that large discrepancies between individual contributions to the bulk

energy tend to cancel out at the level of the total binding energy. We note that nuclear binding energies are indeed prime fit observables constraining parameters of most EDFs.

C. Deformation energy of nuclear LD

The relative LDM contributions of the volume symmetry and surface symmetry energies can be disentangled if shape deformation is present. Indeed, the deformation energy of the deformed LDM can be written as [17,39,94]

$$
\begin{aligned}
E_{\text{def}}^{\text{LDM}} &= E^{\text{LDM}} - E_{\text{sph}}^{\text{LDM}} \\
&= (b_s - 1)a_{\text{surf}}A^{2/3} + (b_{\text{curv}} - 1)a_{\text{curv}}A^{1/3} \\
&\quad + (b_s - 1)a_{\text{ssym}}I^2 A^{2/3} + (b_c - 1)\frac{3}{5}\frac{e^2}{r_0}\frac{Z^2}{A^{1/3}}, \quad (3)
\end{aligned}
$$

where the geometrical factors b_s, b_{curv}, and b_c depend on the shape of the deformed drop (by definition, they are equal to unity at the spherical shape). Since the nuclear volume is conserved in the LDM, the surface and curvature b factors increase with deformation. On the other hand, b_c becomes less than 1 as the Coulomb energy of the deformed drop is lower than that of the spherical drop. While the volume symmetry energy is shape independent, the surface symmetry term has the same dependence on the nuclear shape and A as the surface term. Consequently, these two contributions to the symmetry energy behave differently in deformed nuclear drops.

As an example, in Fig. 3, we plot the individual contributions to $E_{\text{def}}^{\text{LDM}}$ for the two $A = 100$ drops at a fixed quadrupole deformation $\tilde{\beta}_2 = 0.6$. (All remaining deformations are set to zero.) Specifically, shown are contributions from the surface, curvature, Coulomb, and surface symmetry terms corresponding to different Skyrme EDFs. The Coulomb radius r_0 was assumed to be the same as the Wigner-Seitz radius defining the saturation density.

Since, for ^{100}Sn, the isospin excess is zero, the deformation energy contribution coming from the surface symmetry term vanishes. The variations of the total LDM energy between different EDF parametrizations are relatively small and primarily related to slightly different values of a_{surf}. The picture changes dramatically when going to ^{100}Zn, a very neutron-rich nucleus with isospin $I = 0.4$. The variations between predictions of different EDFs have a much larger amplitude and are caused almost exclusively by the surface symmetry term. This indicates that the theoretical differences in the LDM deformation energy of heavy neutron-rich nuclei are almost entirely driven by the poorly determined surface symmetry term. As is clear from Fig. 3, an experimental access to this term can be provided by extracting shell energy from the measured masses of very deformed configurations in neutron-rich nuclei. Another interesting observation drawn from the deformed LDM exercise is that, contrary to the usual scenario in which the macroscopic deformability is solely driven by the competition between surface and Coulomb terms, the macroscopic deformation energy of very neutron-rich nuclei involves a three-way competition between the repulsive surface term and the attractive Coulomb and surface symmetry terms.
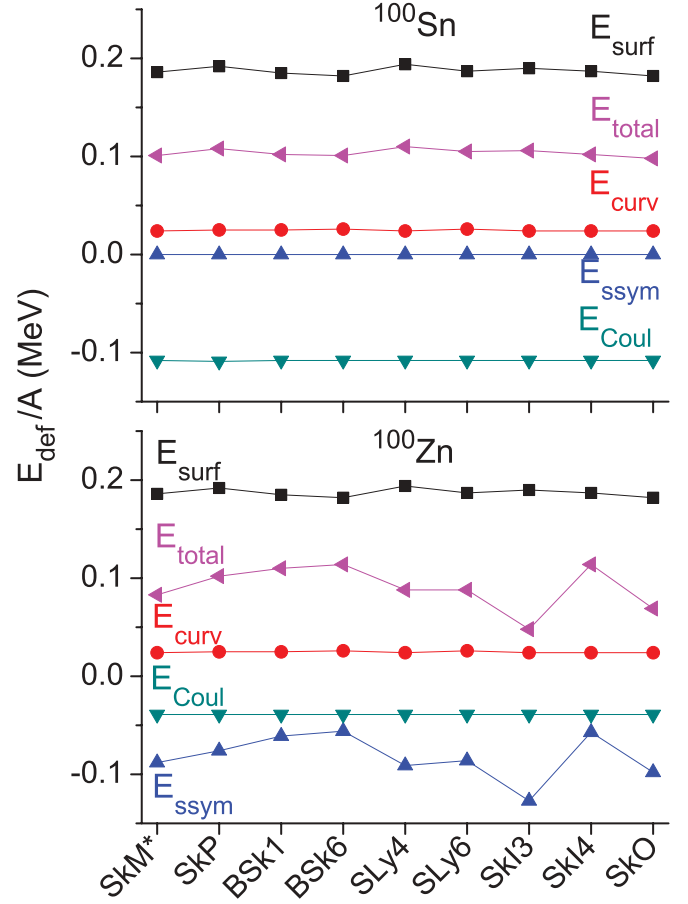

FIG. 3. (Color online) Individual contributions to the total deformation energy per nucleon of the microscopic LDM for nine Skyrme EDFs for two $A = 100$ isobars: ^{100}Sn ($I = 0$, top) and ^{100}Zn ($I = 0.4$, bottom). The assumed quadrupole deformation is $\tilde{\beta}_2 = 0.6$.

III. SKYRME HFB CALCULATIONS AT LARGE DEFORMATIONS

The binding energy of a deformed nuclear configuration can be decomposed into a macroscopic part and shell correction. To determine whether the macroscopic features related to the surface symmetry energy, identified in Sec. II C, show up in self-consistent DFT calculations for actual nuclei, we have performed HFB calculations for a number of states at large deformation with available experimental information.

A. Survey of SD band heads and fission isomers

We selected two regions of the nuclear chart: In the actinides, there is a number of isotopes where the excitation energy of the fission isomer is relatively well known [95]. In the neutron-deficient Hg and Pb isotopes, the linking transition between the SD and the g.s. bands has been identified for several nuclei so that the energy of the 0^+ band head could be extracted [96–101]. All SD band-head data used in this paper are listed in Table II.

HFB calculations were performed with the DFT solvers HFBTHO [102] and HFODD [103–107]. To benchmark binding

TABLE II. Experimental energies of 0^+ band heads of SD states in $A = 190$ mass region and in the actinides.

Nucleus	$E_{SD}(0^+)$ (MeV)	References
^{192}Hg	5.3 (9)	[98]
^{194}Hg	6.017	[97]
^{192}Pb	4.011	[96]
^{194}Pb	4.643	[99]
^{196}Pb	5.630(5)	[101]
^{236}U	2.750	[95]
^{238}U	2.557	[95]
^{240}Pu	2.800	[95]
^{242}Cm	1.900	[95]

energies of SD configurations, we employed several Skyrme EDFs in the particle-hole channel. Pairing correlations were modeled by a mixed-pairing interaction with a dependence on the isoscalar density [108,109]. All calculations were performed with a cutoff energy of $E_{cut} = 60$ MeV to truncate the quasiparticle space. For each parametrization of the Skyrme interaction, the pairing strength was fitted to the average neutron pairing gap in ^{120}Sn according to the procedure described in Ref. [108]. In both solvers, the quasiparticle solutions to the HFB problem are expanded on the deformed harmonic oscillator (HO) basis. Since we are probing very elongated systems, we performed the calculations using a stretched basis with a large number of deformed HO shells, $N_{max} = 20$. All calculations were performed assuming axial reflection symmetric shapes. The constrained minimization was performed using the augmented Lagrangian method [110] and the procedure of Refs. [111,112].

As an illustration of typical deformation landscapes in the two regions, Fig. 4 shows the calculated potential energy curves for ^{194}Pb and ^{236}U as functions of the quadrupole deformation β extracted from the mass quadrupole moment $\langle \hat{Q}_{20} \rangle$ and the total rms radius:

$$\beta \equiv \sqrt{\frac{\pi}{5}} \frac{\langle \hat{Q}_{20} \rangle}{\langle r^2 \rangle}. \tag{4}$$

While the actinide nuclei of interest are always predicted to have prolate-deformed g.s.s with $\beta_2 \approx 0.3$, neutron-deficient Hg and Pb isotopes show a more complex g.s. pattern involving coexisting oblate and spherical structures [113].

The predicted excitation energy of the SD minimum relative to the g.s., $E^*_{th} = E_{SD} - E_{g.s.}$, between the HFB SD minimum and the g.s. minimum can be compared with the experimental value E^*_{exp}. The residuals $\Delta E = E^*_{th} - E^*_{exp}$ are plotted in Fig. 5 for 22 different Skyrme EDFs. It is rather striking to notice that, for a given nucleus, the differences between various EDFs can be as high as 4 MeV, which is often greater than the excitation energy itself. These large fluctuations sometimes occur within a family of Skyrme EDFs (e.g., SLy[x]) and have been explained in some cases by the different recipes to treat the center of mass [114]. In contrast, the Brussels-Montreal parametrizations Bsk[x] and Msk[x] are more consistent with one another. An appreciable EDF dependence for SD states had already been pointed
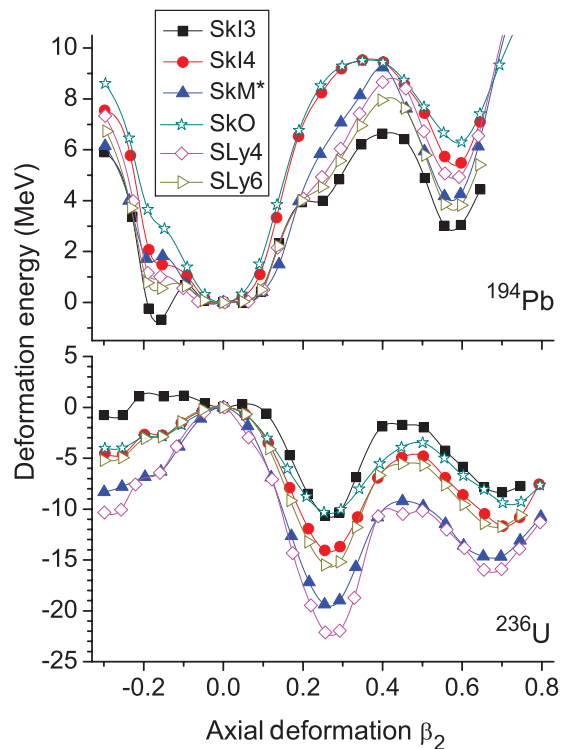

FIG. 4. (Color online) Potential energy curves for ^{194}Pb (top) and ^{236}U (bottom) versus quadrupole deformation β calculated with SkI3, SkI4, SkM*, SkO, SLy4, and SLy6 Skyrme EDFs. All curves are normalized to the spherical point. Axial symmetry is assumed.

out in previous Refs. [115,116]. Similarly, the sensitivity of fission barriers on EDF parametrizations was studied in Refs. [117–119]. In the context of this paper, it is especially interesting to point out that the surface symmetry term has been claimed [118] to have a significant influence on self-consistent fission barriers.

The large spread in calculated values of E^* comes as little surprise: Very few EDFs have been optimized by considering data probing large deformations. The importance of considering strongly deformed shapes when fitting the coupling constants of EDFs was discussed in Refs. [32,84,120], but this program has been carried out only in a handful of cases. The SkM* functional [84] has been fitted by considering the experimental fission barrier in ^{240}Pu. The D1S Gogny interaction [78,121] was also optimized for fission properties. In the Bsk14 EDF of the HFB-14 mass model [122], data on fission barriers were utilized to optimize the EDF parameters by adding a phenomenological collective correction accounting for the zero-point rotational-vibrational motion. In this paper, we do not employ zero-point corrections as we are primarily interested in the deformation properties of the functionals themselves. We refer, for example, to Ref. [123] for a more thorough discussion of dynamical correlations and their impact on deformation properties of nuclei. We note, in passing, that such correlations are supposed to impact standard DFT predictions of g.s. energies of Hg and Pb nuclei because of coexistence effects [124,125].
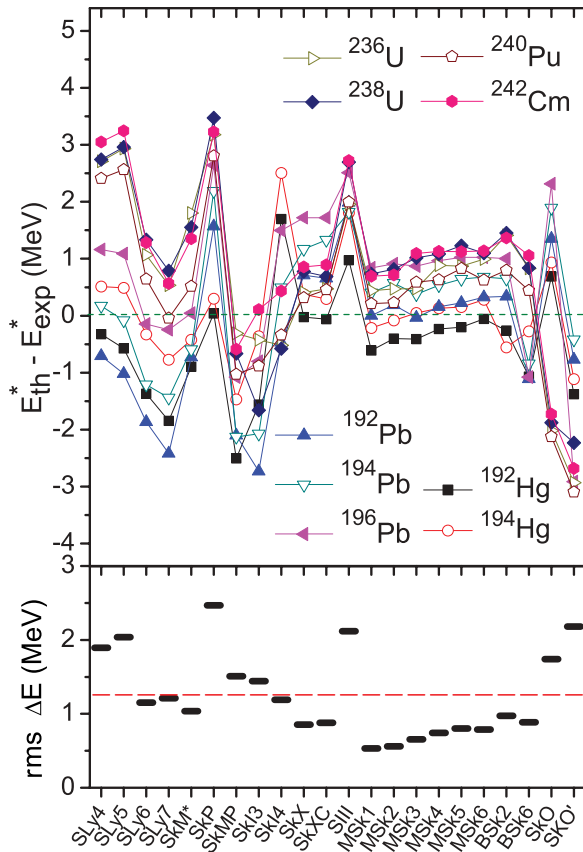
FIG. 5. (Color online) Residuals $\Delta E = E^*_{th} - E^*_{exp}$ (top) and rms deviations from experiment (bottom) for various Skyrme EDFs. Additional references for the Skyrme forces: SLy5-SLy7 [88], SkMP [126], SkX-SkXC [127], SIII [128], MSk1-MSk6 [129], BSk2 [87], SkO' [90]. The average rms deviation for the set of EDFs considered (marked by a dashed line in the lower panel) is 1.26 MeV for the nine data points of Table II and 1.34 MeV for the fission isomers nuclei.

B. Estimation of theoretical errors

Since the values of ΔE in Fig. 5 are subject to numerical and experimental uncertainties, it is important to estimate their respective errors before assessing the model dependence of results. To validate E^*_{th}, we studied the convergence of our HFB results with respect to the size of HO space used. Figure 6 shows the HFB + SkM* energy of the g.s. and SD state of ^{240}Pu calculated with the HFBTHO solver as a function of N_{max}, The HFBTHO numbers are compared to the benchmark results obtained with the precise coordinate-space DFT solver HFB-AX [130].

With the large HO basis used here ($N_{max} = 20$), the theoretical error on the energy of either the g.s. or the SD state is around 600 keV. Since the HFB theory is variational, the error on the excitation energy, in fact, is much smaller (see the bottom panel of Fig. 5), and comes principally from the different convergence rates of HFB states with $\beta_2 \approx 0.3$ and $\beta_2 \approx 0.6$. Those differences are caused by the combination of effects coming from the basis deformation and the choice of oscillator frequency $\hbar\omega$. At $N_{max} \geqslant 16$, the dependence on $\hbar\omega$ is rather weak; hence, the only remaining source of fluctuations
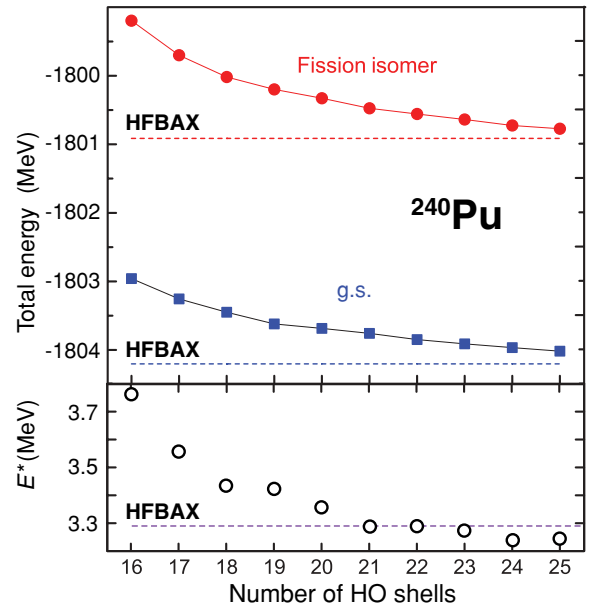

FIG. 6. (Color online) Convergence of the HO basis expansion for the HFB + SkM* binding energy of the fission isomer and g.s. (top panel) and the excitation energy of the fission isomer (bottom panel) in ^{240}Pu as a function of the HO basis size. Results are compared with the benchmark numbers obtained with the precise coordinate-space solver HFB-AX [130].

is the basis deformation. For the residuals, we estimate the latter empirically to be at most 500 keV for 16 shells and less than 100 keV for $N_{max} \geqslant 16$ shells.

The convergence pattern of HFB calculations seen in Fig. 6 is, to a large extent, exponential. A similar behavior has also been observed in *ab initio* calculations of Refs. [131–133]. However, in all these many-body approaches, the size of the actual model space grows combinatorially with the number of active particles and single-particle states taken, which is not the case for DFT. In a recent work, the exponential convergence of wave functions expanded in a HO basis, in fact, has been related to its weak differentiability properties [134]. It has been argued therein that this may be a generic property of systems with exponentially decaying wave functions.

For all the nuclei considered in Fig. 6 and Table II, experimental g.s. masses are known to an excellent precision of approximately 2 keV [135]. In the $A \sim 190$ region, the uncertainty of the SD band head comes from the extrapolation of the rotational band down to spin 0^+. This procedure is slightly model dependent, but its error is estimated to be only ~ 5 keV [96–101]. In the actinides, the determination of the excitation energy of the fission isomer is slightly less precise: It is about 5–10 keV for ^{236,238}U and about 200 keV for ^{240}Pu and ^{242}Cm [95].

Considering the foregoing, the theoretical fluctuations of approximately several MeV in ΔE seen in Fig. 5 are well above numerical uncertainties in E^*_{th} and experimental uncertainties in E^*_{exp}. Consequently, these deviations are rooted in actual EDF parametrizations. In Sec. IV, we will investigate the

relation between the fluctuations in ΔE and the underlying LDM description.

IV. BULK DEFORMATION ENERGY OF THE SKYRME EDF

To extract the smooth LDM energy from HFB results, the fluctuating contributions to the energy (i.e., shell-correction and pairing terms) must be removed. After describing the details of the extraction technique employed, we show how the leptodermous expansion of the smoothed HFB energy works.

A. Pairing and shell corrections

To extract shell and pairing corrections from the total HFB energy is not an easy task as the building blocks of HFB are quasiparticles rather than the single-particle states that enter the Strutinsky energy theorem [22]. Moreover, while the contribution of pairing correlations to the total energy must be eliminated, the induced shape polarization must be kept as is relevant for performing the direct comparison with experiment.

To extract the effect of HFB pairing, we carried out HF calculations at the equilibrium deformations of HFB g.s. and SD configurations. This was achieved by constraining the expectation values of the HF multipole moments at those corresponding to HFB solutions. In practice, it sufficed to consider $\hat{Q}_{20}$, $\hat{Q}_{40}$, $\hat{Q}_{60}$, and $\hat{Q}_{80}$ moments, higher-order terms being negligible. The advantages of this procedure are twofold. First, it enables us to remove all direct pairing effects. Second, it provides a set of single-particle HF states that can be used to compute the shell correction δE_{shell}.

Shell corrections were calculated according to the procedure outlined in Refs. [82,83]. It combines the standard shell-correction smoothing method (our original implementation is based on Ref. [17]) with the Green's function oscillator expansion method technique that is aimed at removing the spurious contribution to δE_{shell} stemming from the nonresonant continuum of positive-energy states. Following Ref. [81], we employed the following smoothing parameters: smoothing widths $\gamma_n = 1.66$ for neutrons and $\gamma_p = 1.54$ for protons (in units of $\hbar\omega_0 = 41/A^{1/3}$) and the curvature correction $p = 10$. This choice guarantees that the generalized plateau condition is satisfied [82].

As an illustration, Fig. 7 shows the smooth single-particle density $\tilde{g}(e)$ for protons in the g.s. and fission isomer of ^{240}Pu obtained with SkM* EDF. The generalized plateau condition requires that this function must be linear across several oscillator shells, and this is indeed well fulfilled. Figure 8 displays the convergence of the shell-correction contribution to the deformation energy, $\delta E_{\text{shell}}^{\text{SD}} - \delta E_{\text{shell}}^{\text{g.s.}}$, as a function of N_{max}. While the convergence is not perfect, the uncertainty remains fairly small, around 200 keV.

We should emphasize that there exist alternative ways to extract shell correction, see, for example, Refs. [73,136]. However, since we use LDM parameters extracted in Ref. [27] by employing the Green's function prescription [82], it is important to follow the same procedure for our analysis to remain consistent.
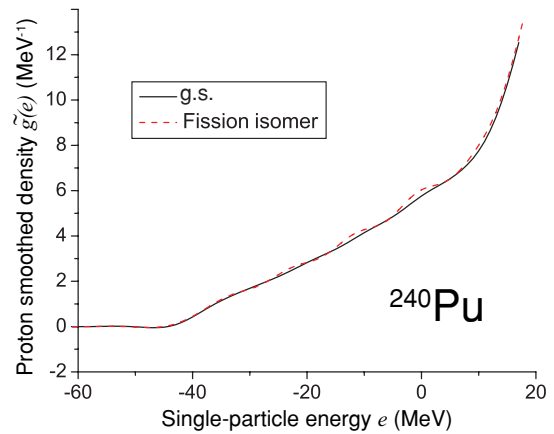

FIG. 7. (Color online) Proton smoothed single-particle density $\tilde{g}(e)$ in the g.s. and SD configuration of ^{240}Pu calculated with the SkM* EDF and $N_{\text{max}} = 16$ HO shells.

B. Determination of microscopic LDM deformations

To compare the LDM deformation energy with the HFB bulk energy, one needs to properly define the shape of the (sharp) surface of the drop. For the axial reflection symmetric shapes considered in this paper, the drop surface is typically parametrized in terms of deformations $\tilde{\beta}_l$ defining the multipole expansion of the drop radius. Therefore, the problem consists of mapping a set $\{\tilde{\beta}_l\}_{l=2,4,\ldots,N_Q}$ to a set of multipole moments $\langle \hat{Q}_\lambda \rangle^{\text{HF}} = \langle r^\lambda Y_{\lambda 0} \rangle$ coming from HF calculations.

The LDM deformation parameters $\tilde{\beta}_l$ can be determined from the system of nonlinear equations [137],

$$\langle \hat{Q}_\lambda(\tilde{\beta}_l) \rangle = \langle \hat{Q}_\lambda \rangle^{\text{HF}}, \quad \lambda = 0, 2, 4, \ldots, N_Q. \quad (5)$$

However, in such an approach involving standard (volume) multipole moments, the role of higher-order multipoles becomes artificially exaggerated. Therefore, it was argued (see Refs. [138,139] and references quoted therein) that a mapping between the two sets of shape deformations can be best
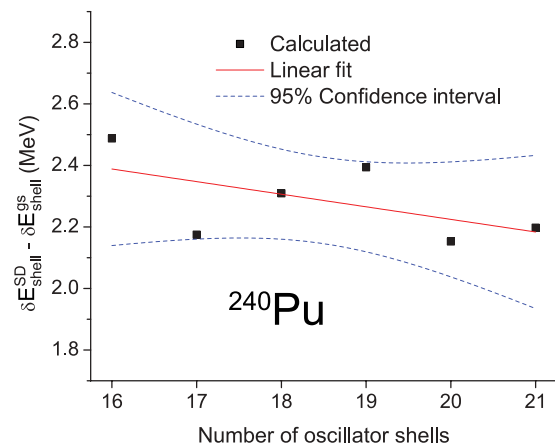

FIG. 8. (Color online) Convergence of the shell-correction contribution to the deformation energy, $\delta E_{\text{shell}}^{\text{SD}} - \delta E_{\text{shell}}^{\text{g.s.}}$, for ^{240}Pu as a function of N_{max}. Calculations were performed with with the SkM* EDF.

achieved by using the surface multipole moments defined as $\hat{Q}_\lambda \equiv r^2 Y_{\lambda 0}$, which have a much softer radial dependence than volume moments. Therefore, deformation parameters $\tilde{\beta}_l$ can be extracted by requiring that the set of equations for dimensionless surface moments [138,139],

$$\frac{\langle \hat{Q}_\lambda(\tilde{\beta}_l) \rangle}{\langle r^2(\tilde{\beta}_l) \rangle} = \frac{\langle \hat{Q}_\lambda \rangle^{\mathrm{HF}}}{\langle r^2 \rangle^{\mathrm{HF}}} \tag{6}$$

be satisfied, with $l, \lambda = 2, \ldots, N_Q$. In practice, only the four lowest terms with $l = 2, 4, 6, 8$ are important at SD shapes. This choice provides the best mapping between self-consistent multipole moments and deformations of the sharp surface.

C. Coulomb polarization

In Ref. [27], the microscopic LDM parameters were extracted from a set of spherical HF calculations without the Coulomb term. However, such a methodology is clearly not applicable in realistic calculations. First, the Coulomb term crucially affects nuclear deformability. Second, while its contribution to the total energy can easily be subtracted, the Coulomb potential induces a long-range polarization of the mean field, which affects the equilibrium deformations, single-particle states, etc. Most importantly, this Coulomb polarization is deformation dependent. As a result, the contribution of the Coulomb term to the excitation energy, E^*_{Cou}, can vary by up to several MeV for the interactions that we consider in this paper.

To take this effect into account at the LDM level, we first extract the spherical charge radius $R_0^{\mathrm{ch}} = r_0^{\mathrm{ch}} A^{1/3}$ from the self-consistent spherical HF calculations for each nucleus (Z, N) and then use this value of r_0^{ch} in Eq. (3). Thus, since the charge radius obtained does not come from a systematic fit but is obtained locally, it introduces shell fluctuations into LDM. However, since spherical self-consistent radii behave smoothly as a function of shell filling [140], the corresponding shell effect is very small indeed.

Our actual determination of the LDM charge radius goes as follows. From the spherical rms proton HF radius $\langle R_p^2 \rangle$, we extract the rms charge radius $\langle R_{\mathrm{ch}}^2 \rangle$ according to the standard formula

$$\langle R_{\mathrm{ch}}^2 \rangle = \langle R_p^2 \rangle + \langle r_p^2 \rangle + \frac{N}{Z} \langle r_n^2 \rangle, \tag{7}$$

where $\langle r_p^2 \rangle = 0.764\ \mathrm{fm}^2$ and $\langle r_n^2 \rangle = -0.116\ \mathrm{fm}^2$ are the squared rms proton and neutron charge radii, respectively. The geometrical charge radius R_0^{ch} is then obtained from the rms charge radius in the usual way:

$$R_0^{\mathrm{ch}} = \frac{5}{3} \sqrt{\langle R_{\mathrm{ch}}^2 \rangle}. \tag{8}$$

We note that the condition $(R_{\mathrm{ch}}^2)^{\mathrm{LD}} = \langle R_{\mathrm{ch}}^2 \rangle^{\mathrm{HF}}$ together with Eq. (6) implies that the charge surface of the microscopic LD is close to that of HF.
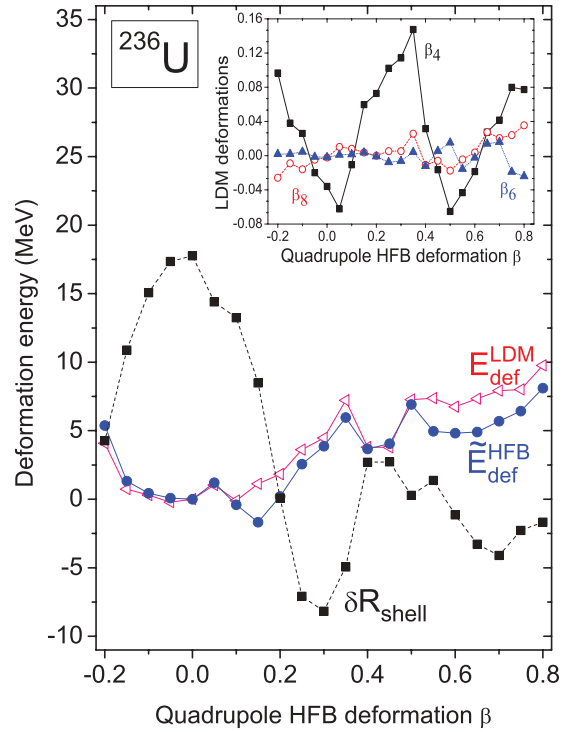

FIG. 9. (Color online) Extraction of the LDM deformation energy from constrained HF + SLy4 calculations for ^{236}U at several values of quadrupole deformation β. Shown are the total shell correction $\delta E_{\mathrm{shell}}$ (squares), the smooth HFB deformation energy $\tilde{E}_{\mathrm{def}}^{\mathrm{HF}}(\beta)$ (dots), and the corresponding LDM deformation energy $E_{\mathrm{def}}^{\mathrm{LDM}}(\beta)$ (triangles). The inset shows the equivalent LDM deformations $\tilde{\beta}_l$ with $l = 4, 6,$ and 8.

D. Example: Extraction of the smooth deformation energy for ^{236}U

To illustrate the extraction procedure of smooth deformation energy from HF results and to assess the quality of the leptodermous expansion, we carry out constrained HF + SLy4 calculations for ^{236}U shown in Fig. 9. The constraint on the quadrupole moment was determined so that the deformation β of Eq. (4) takes the values $\beta = -0.20, -0.15, \ldots, +0.80$. Since the HF potential energy curve consists of several sharply crossing configurations as evidenced by rapidly varying LDM deformations shown in the inset of Fig. 9, we made no attempt to interpolate between the mesh points in β. The shell correction was extracted at each β according to the procedure discussed in Sec. IV A. The smooth energy at deformation β is given by $\tilde{E}^{\mathrm{HF}}(\beta) = E^{\mathrm{HF}}(\beta) - \delta E_{\mathrm{shell}}(\beta)$, which defines the smooth component of the HF deformation energy $\tilde{E}_{\mathrm{def}}^{\mathrm{HF}}(\beta) = \tilde{E}^{\mathrm{HF}}(\beta) - \tilde{E}^{\mathrm{HF}}(\beta = 0)$. At each β, the LDM deformation parameters $\tilde{\beta}_l$ are computed according to Sec. IV B. Finally, the deformed LDM energy $E_{\mathrm{def}}^{\mathrm{LDM}}(\beta)$ is obtained using Eq. (3) with the LDM constants corresponding to the SLy4 interaction taken from Table I and the charge radius defined according to Sec. IV C. As expected, the smooth deformation energy is growing as a function of deformation; the local variations are caused by configuration changes in HF calculations and corresponding changes in higher-order shape deformations.

Although the agreement between $E_{\rm def}^{\rm LDM}$ and $\tilde{E}_{\rm def}^{\rm HF}$ is not perfect, it is gratifying to see that the LDM energy nicely follows the smooth energy extracted from HFB. The deviation has multiple sources, such as the error on the regression analysis carried in Ref. [27], uncertainties of the shell-correction procedure, neglect of the second-order effects in density fluctuations [22], LDM assumption of the sharp surface, limitations of the leptodermous expansion used, etc. Considering all this, the quality of the leptodermous expansion of the deformation energy in deformed nuclei is very reasonable.

V. SURFACE SYMMETRY ENERGY AND DEFORMED NEUTRON-RICH NUCLEI IN DFT

We are now ready to determine the smooth part of the deformation energy from HFB results and to compare it with the microscopic LDM using the methodology described in Sec. IV. In Fig. 3, we demonstrated that the uncertainties in the determination of $a_{\rm ssym}$ impact the deformation properties of neutron-rich nuclear drops. Therefore, it is interesting to see whether, in the studies of well-deformed states in realistic nuclei, these uncertainties would show up.

Figure 10 shows the smooth excitation energy $\tilde{E}^*$ of fission isomers calculated in HFB and LDM for seven EDFs. For each nucleus, we first carried out HFB calculations to determine the g.s. and SD configurations. The constrained HF calculations are then performed based on the multipole moments of the HFB solution. Shell energies are subtracted from g.s. and SD HF energies, and this defines the smooth part of the excitation energy $\tilde{E}_{\rm HFB}^*$ in HFB (i.e., the smooth deformation energy of the excited state relative to the g.s.). By using the surface moments obtained in the g.s. and SD minima of HFB, we extract the equivalent LDM deformation parameters $\tilde{\beta}_l$ and the LDM excitation energy.

As in Sec. III, clear differences between various EDF parametrizations can be seen. Overall, these variations can
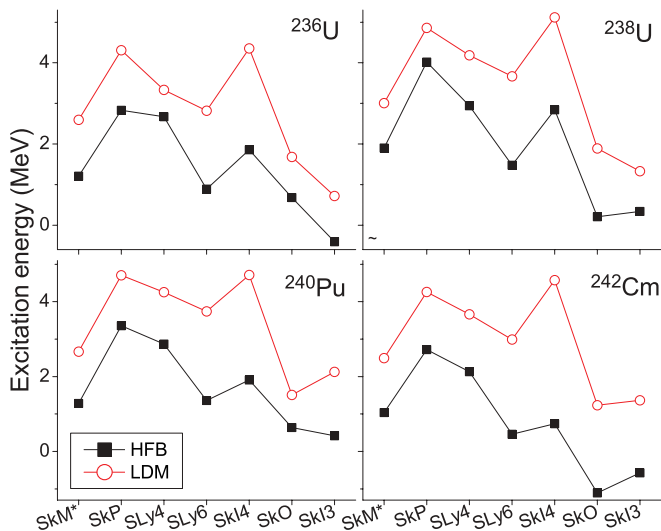

FIG. 10. (Color online) Smooth excitation energy $\tilde{E}^*$ of fission isomers in ^{236,238}U, ^{240}Pu, and ^{242}Cu calculated in HFB and LDM for seven EDFs. See text for details.
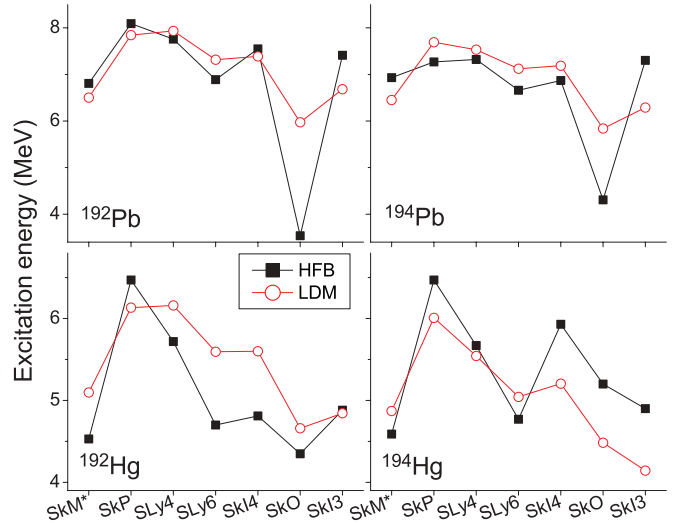

FIG. 11. (Color online) Same as in Fig. 10 except for SD band heads in ^{192,194}Hg and ^{192,194}Pb.

be as large as 4 MeV at the LDM level. As discussed earlier in Sec. IV D, there is an $\sim 2-$MeV shift of the LDM curves with respect to the HFB results. However, it is rewarding to see that the shift is systematic and the EDF variations seen in HFB are properly captured by the equivalent LDM. The results for the SD band heads are displayed in Fig. 11. In these lighter nuclei, the agreement between HFB and equivalent LDM is better on average, but local fluctuations can be appreciable (see SkO or SkI3 results for Pb isotopes) and might be related to a complex pattern of g.s. equilibrium deformations in these nuclei.

The results shown in Figs. 10 and 11, combined with the overall picture of the residuals in Fig. 5, demonstrate that large differences between Skyrme EDFs exist when it comes to deformation properties of nuclei. While these differences certainly depend on variations of EDF parameters controlling the shell structure, such as, for example, the effective mass or spin-orbit splitting, our analysis indicates that there are also fundamental discrepancies at the level of the bulk energy. Therefore, one may question whether EDF optimization protocols based exclusively on a small amount of data in nuclear matter and spherical nuclei are able to capture the deformability of EDF.

As discussed in Sec. II and, in particular, in Figs. 1 and 2, $a_{\rm ssym}$ varies very significantly from one EDF to another. Consequently, surface and symmetry properties of EDFs are intertwined in a nontrivial way when it comes to deformability. Guided by the results of Figs. 10 and 11, we may wonder whether the large variations in $a_{\rm ssym}$ are indeed reflected in the results of self-consistent calculations.

Figure 12 shows the surface and surface symmetry contributions to the LDM excitation energy of SD states in the actinides for the same Skyrme EDFs as in Figs. 10 and 11. The equilibrium deformations that are used in the LDM for both the g.s. and the SD state are obtained in HFB. The LDM results are compared to the smooth HFB energy $\tilde{E}_{\rm HFB}^*$. To facilitate interpretation, all curves are normalized to SkM* values. In this way, we can better compare relative variations obtained in various EDFs. It is interesting to see that the inter-EDF
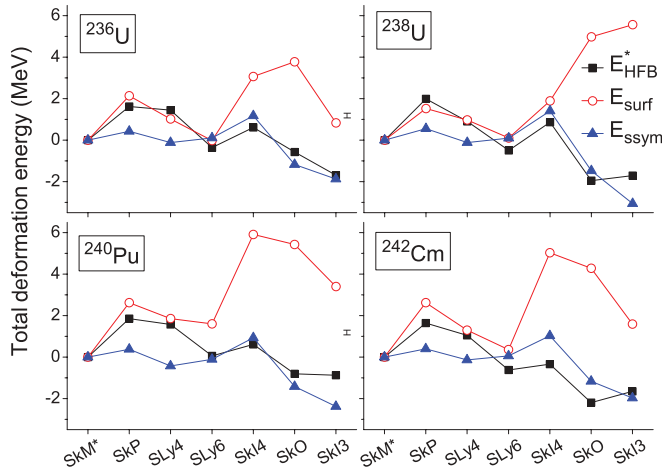
FIG. 12. (Color online) Surface and surface symmetry contributions to the LDM excitation energy of fission isomers in the actinides compared to the smooth HFB excitation energy for the same Skyrme EDFs as in Figs. 10 and 11. All curves are shown relative to SkM* results.

FIG. 13. (Color online) Quadrupole deformations β in SkM* for g.s.s and fission isomers in a sequence of neutron-rich U isotopes (top) and the corresponding excitation energies (bottom).

fluctuations of $\tilde{E}_{HFB}^*$ are rather well correlated with the surface symmetry energy. In other words, the contribution from the Coulomb and curvature terms (not plotted in Fig. 12 for better legibility) cancel out the surface term to a large extent. This result is significant because it seems to confirm the simple analysis of Sec. II in a realistic case: In nuclei having large neutron excess I (here, on the order of $I \approx 0.2$), differences in deformation energy between various EDF parametrizations reflect the differences of the surface symmetry coefficient. In contrast, a similar analysis of individual macroscopic contributions in the Hg-Pb region does not allow pinning down a single LDM term as a primary deformation driver.

To further illustrate the importance of the surface symmetry term, we calculated the LDM excitation energy of the fission isomer for a sequence of U isotopes. Here, we employed the SkM* and BSk6 parametrizations. The SkM* EDF is known to perform rather well for fission barriers [141,142]. Its surface symmetry coefficient is also close to the average among Skyrme forces and values from phenomenological estimates, so it can be viewed as fairly representative of the Skyrme functionals. The BSk6 parametrization gives a reasonable rms deviation for excitation energies of SD states, see Fig. 5. The isotopes considered include some very neutron-rich species important in the context of r-process fission recycling. It is worth noting that HFB potential energy landscapes change considerably within this isotopic sequence. For example, $N = 184$ is a neutron magic number for SkM* [81]; hence, g.s. configurations around ^{276}U are spherical rather than prolate, see Fig. 13. Therefore, the equivalent LDM equilibrium deformations reflect these structural changes in a nontrivial way.

For each isotope, we computed the relative contribution of the surface, surface symmetry, curvature, and Coulomb term to the total LDM excitation energy: These are the only terms that depend on deformation. Figure 14 shows the percentage of the LDM excitation energy from these
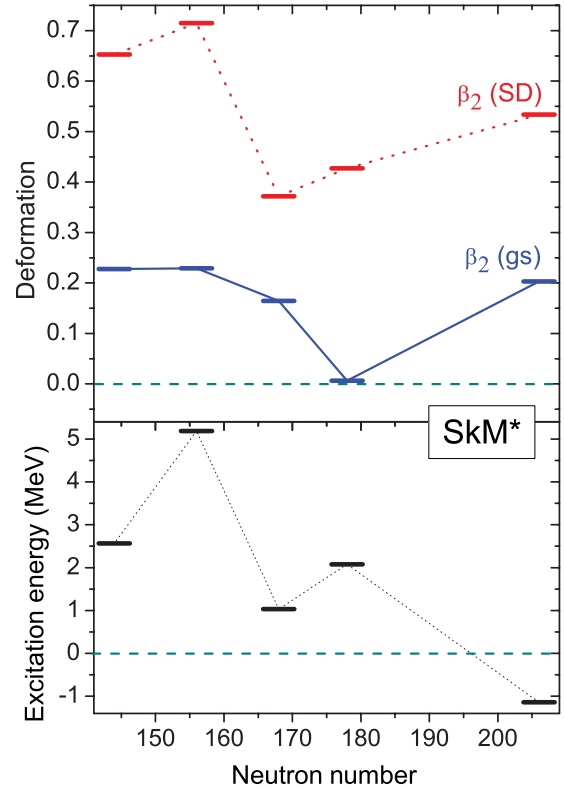
contributions. As the neutron excess grows, one can notice the gradual relative decrease of the Coulomb contribution—which depends only on the number of protons and proton density and, therefore, remains relatively constant in value. This decrease is compensated by an increase of the surface symmetry contribution. For the most neutron-rich nuclei considered here, the total contribution from E_{ssym} is as large as 19% for SkM*. For the two parametrizations selected here, the role of the
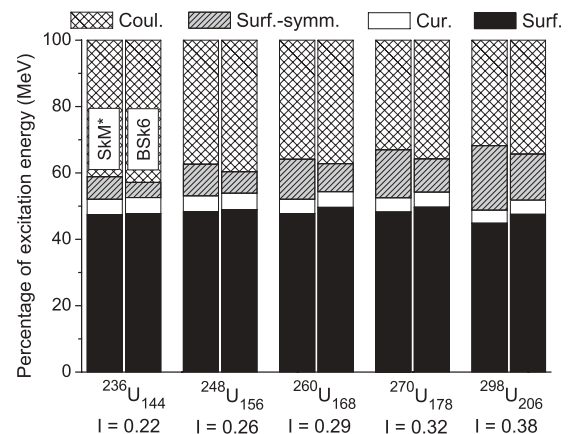

FIG. 14. Relative contributions of the Coulomb, surface symmetry, curvature, and surface terms to the equivalent LDM excitation energy of fission isomers for the same U isotopes as in Fig. 13. Calculations are based on SkM* and BSk6.

surface symmetry term increases by a factor of 3 from ^{236}U to the fission recycling region.

VI. CONCLUSIONS

This paper contains a comprehensive study of deformation properties of nuclear EDFs based on the leptodermous expansion of the smooth nuclear energy. Since symmetry and surface symmetry terms in the expansion are strongly correlated, a way to resolve them is to consider data on deformed neutron-rich nuclei in which the surface symmetry term is amplified. Based on intuitive LDM arguments, we argue that deformation properties of neutron-rich nuclear drops are governed by an interplay of the deformation-driving Coulomb and surface symmetry terms and the surface energy that acts against shape deformation. To estimate this interplay, we extracted the smooth deformation part of the HFB energy by means of the shell-correction procedure.

Self-consistent DFT calculations for excitation energies of SD states show marked differences in their predictions depending on the parametrization used. For the set of EDFs considered, the average rms deviation between predicted energies of SD states and experimental values is 1.26 MeV. Within this set, the MSk1 parametrization provides the best overall reproduction of the data: The corresponding rms deviation is 0.53 MeV, and this sets a benchmark for future improvements. For the subset of fission isomer data, the best performer is SkI4: Its rms deviation is 0.48 MeV.

We showed that interparametrization differences reflect, to a large extent, macroscopic properties of EDFs. In particular, our calculations indicate that the bulk deformation properties of actinides are strongly driven by surface symmetry effects, while in the proton-rich $A \sim 190$ nuclei, there is more competition between the various macroscopic contributions. This finding should have an impact on the fissility of heavy very neutron-rich nuclei of the kind encountered, for example, in the r process. For example, the surface symmetry contribution to the bulk part of the excitation energy of fission isomer in very neutron-rich uranium isotopes can reach $\sim 20\%$ as compared with $\sim 5\%$ for ^{236}U.

The importance of the surface symmetry term on fission can be quantified at the LDM level by the dimensionless fissility parameter,

$$ x = \frac{E_{\mathrm{Coul}}(\mathrm{sph})}{2E_{\mathrm{surf}}(\mathrm{sph})} \approx \frac{Z^2}{47A(1 - \eta I^2)}, \tag{9} $$

where $\eta \equiv -a_{\mathrm{ssym}}/a_{\mathrm{surf}}$. If $x > 1$, the nuclear LD is unstable for fission. In the presence of neutron excess, the fissility parameter increases (i.e., the tendency toward fission increases). In Refs. [56,143], the value $\eta = 1.7826$ was used. By taking LDM parameters from Table I, we see that η is 1.9 for BSk6, 2.9 for SkM*, and 4.16 for SkI3 (i.e., this parameter is very uncertain).

Figure 15 shows the LDM fission limit for the SkI3 and SkM* EDFs as well as for $\eta = 1.7826$ and $\eta = 0$ (no isospin dependence). The minimum value obtained for Z^2/A [i.e., 47 in Eq. (9)] is not very precise as it depends on assumptions about the LDM constants [144]. Therefore, this diagram should
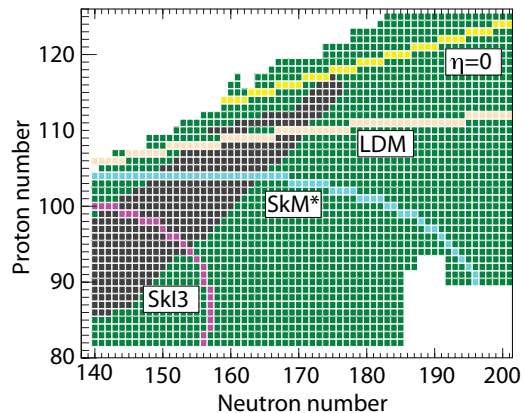

FIG. 15. (Color online) The upper part of the chart of the nuclides with the $x = 1$ limit indicated for SkI3 and SkM* EDFs, the value of $\eta = 1.7826$ used in Ref. [143] (LDM), and no isospin dependence ($\eta = 0$). The region of known nuclides is marked by black squares.

be considered as a qualitative guidance. A clear message drawn from Fig. 15 is that the surface symmetry term can significantly impact LDM fission barriers: The greater the value of η, the lower the threshold for fission. This result is especially important in the context of the fission recycling mechanism in the r process and hot fission reactions leading to excited neutron-rich superheavy nuclei. Since shell effects are, to a large extent, washed out at high temperatures [16,145], the fission of hot compound nuclei is expected to be governed by the LDM fission barrier (or smooth HFB deformation energy). As seen in Fig. 15, the uncertainty in a_{ssym}, hence, η makes it difficult to reliably predict fission rates of the heaviest and superheavy neutron-rich nuclei. (In this context, we note that, according to the recent estimates [146], a_{ssym} and η are expected to depend very weakly on temperature.)

The results obtained in this paper suggest that adding to the list of fit-observables data on strongly deformed nuclear states (such as excitation energies of SD states or fission barriers), combined with the usual constraints on bulk properties and shell structure, should constrain the surface properties of the nuclear EDF quite effectively. Such a strategy is currently being pursued within the Universal Nuclear Energy Density Functional (UNEDF) project [147,148]. On the experimental side, new information on deformed properties on neutron-rich systems is the key.

[1] M. Bender, P.-H. Heenen, and P.-G. Reinhard, Rev. Mod. Phys. **75**, 121 (2003).

[2] J. R. Stone and P.-G. Reinhard, Prog. Part. Nucl. Phys. **58**, 587 (2007).

[3] F. Chappert, M. Girod, and S. Hilaire, Phys. Lett. B **668**, 420 (2008).

[4] P. Klüpfel, P.-G. Reinhard, T. J. Bürvenich, and J. A. Maruhn, Phys. Rev. C **79**, 034310 (2009).

[5] S. Goriely, N. Chamel, and J. M. Pearson, Phys. Rev. C **82**, 035804 (2010).

[6] J. Dobaczewski and W. Nazarewicz, Philos. Trans. R. Soc. London, Ser. A **356**, 2007 (1998).

[7] J. Dobaczewski and W. Nazarewicz, Prog. Theor. Phys. Suppl. **146**, 70 (2002).

[8] J. Erler, P. Klüpfel, and P.-G. Reinhard, J. Phys. G **37**, 064001 (2010).

[9] G. F. Bertsch, B. Sabbey, and M. Uusnäkki, Phys. Rev. C **71**, 054311 (2005).

[10] M. Kortelainen, J. Dobaczewski, K. Mizuyama, and J. Toivanen, Phys. Rev. C **77**, 064307 (2008).

[11] J. Friedrich and P.-G. Reinhard, Phys. Rev. C **33**, 335 (1986).

[12] J. Toivanen, J. Dobaczewski, M. Kortelainen, and K. Mizuyama, Phys. Rev. C **78**, 034306 (2008).

[13] P.-G. Reinhard and W. Nazarewicz, Phys. Rev. C **81**, 051303(R) (2010).

[14] M. Kortelainen, T. Lesinski, J. Moré, W. Nazarewicz, J. Sarich, N. Schunck, M. V. Stoitsov, and S. Wild, Phys. Rev. C **82**, 024313 (2010).

[15] *Scientific Opportunities with a Rare-Isotope Facility in the United States* (The National Academies Press, Washington, DC, 2007).

[16] M. Brack, J. Damgård, A. S. Jensen, H. C. Pauli, V. M. Strutinsky, and C. Y. Wong, Rev. Mod. Phys. **44**, 320 (1972).

[17] M. Bolsterli, E. O. Fiset, J. R. Nix, and J. L. Norton, Phys. Rev. C **5**, 1050 (1972).

[18] A. Bohr and B. R. Mottelson, *Nuclear Structure* (Benjamin, New York, 1975), Vol. II.

[19] S. G. Nilsson and I. Ragnarsson, *Shapes and Shells in Nuclear Structure* (Cambridge University Press, Cambridge, UK, 1995).

[20] V. M. Strutinsky, Nucl. Phys. A **95**, 420 (1967).

[21] V. M. Strutinsky, Nucl. Phys. A **122**, 1 (1968).

[22] P. Ring and P. Schuck, *The Nuclear Many-Body Problem* (Springer-Verlag, Berlin, 1980).

[23] M. Brack and P. Quentin, Nucl. Phys. A **361**, 35 (1981).

[24] M. Kortelainen, R. J. Furnstahl, W. Nazarewicz, and M. V. Stoitsov, Phys. Rev. C **82**, 011304(R) (2010).

[25] W. D. Myers and W. J. Swiatecki, Ann. Phys. (NY) **55**, 395 (1969).

[26] W. D. Myers and W. J. Swiatecki, Ann. Phys. (NY) **84**, 186 (1974).

[27] P.-G. Reinhard, M. Bender, W. Nazarewicz, and T. Vertse, Phys. Rev. C **73**, 014309 (2006).

[28] P. Danielewicz and Jenny Lee, Nucl. Phys. A **818**, 36 (2009).

[29] M. Farine, J. M. Pearson, and B. Rouben, Nucl. Phys. A **304**, 317 (1978).

[30] M. Farine, J. Côté, and J. M. Pearson, Nucl. Phys. A **338**, 86 (1980).

[31] M. Farine, J. Côté, and J. M. Pearson, Phys. Rev. C **24**, 303 (1981).

[32] F. Tondeur, M. Brack, M. Farine, and J. M. Pearson, Nucl. Phys. A **420**, 297 (1984).

[33] P. Danielewicz, Nucl. Phys. A **727**, 233 (2003).

[34] A. W. Steiner, M. Prakash, J. M. Lattimer, and P. J. Ellis, Phys. Rep. **411**, 325 (2005).

[35] A. E. L. Dieperink and P. Van Isacker, Eur. Phys. J. A **32**, 11 (2007).

[36] M. W. Kirson, Nucl. Phys. A **798**, 29 (2008).

[37] H. S. Köhler, Nucl. Phys. A **258**, 301 (1976).

[38] E. Lipparini and S. Stringari, Phys. Lett. B **112**, 421 (1982).

[39] P. Möller, J. R. Nix, W. D. Myers, and W. J. Swiatecki, At. Data Nucl. Data Tables **59**, 185 (1995).

[40] T. Mukhopadhyay and D. N. Basu, Nucl. Phys. **A789**, 201 (2007).

[41] N. Wang and M. Liu, Phys. Rev. C **81**, 067302 (2010).

[42] P. Danielewicz and J. Lee, AIP Conf. Proc. **947**, 301 (2007).

[43] V. M. Kolomietz and A. I. Sanzhur, Phys. Rev. C **81**, 024324 (2010).

[44] W. Satuła, R. A. Wyss, and M. Rafalski, Phys. Rev. C **74**, 011301(R) (2006).

[45] M. V. Stoitsov, J. Dobaczewski, W. Nazarewicz, S. Pittel, and D. J. Dean, Phys. Rev. C **68**, 054312 (2003).

[46] S. Goriely, N. Chamel, and J. M. Pearson, Phys. Rev. Lett. **102**, 152503 (2009).

[47] C. Y. Wong, Ann. Phys. (NY) **77**, 279 (1973).

[48] J. Dechargé, J.-F. Berger, M. Girod, and K. Dietrich, Nucl. Phys. A **716**, 55 (2003).

[49] Y. Yu, A. Bulgac, and P. Magierski, Phys. Rev. Lett. **84**, 412 (2000).

[50] W. Nazarewicz, M. Bender, S. Ćwiok, P. H. Heenen, A. T. Kruppa, P.-G. Reinhard, and T. Vertse, Nucl. Phys. A **701**, 165 (2002).

[51] F. J. Viñas, M. Centelles, and M. Warda, Int. J. Mod. Phys. E **17**, 177 (2008).

[52] P. Möller, A. J. Sierk, T. Ichikawa, and A. Iwamoto, Prog. Theor. Phys. Suppl. **154**, 21 (2004).

[53] V. Zagrebaev and W. Greiner, Phys. Rev. C **78**, 034610 (2008).

[54] I. V. Panov, I. Y. Korneev, T. Rauscher, G. Martínez-Pinedo, A. Kelic-Heil, N. T. Zinner, and F.-K. Thielemann, Astronomy and Astrophysics **513**, A61 (2010).

[55] W. Nazarewicz, J. Dobaczewski, M. Matev, S. Mizutori, and W. Satuła, Acta Phys. Pol. **32**, 2349 (2001).

[56] A. G. W. Cameron, Astrophys. J. **587**, 327 (2002).
[57] I. V. Panov, I. Yu. Korneev, and F.-K. Thielemann, Astron. Lett. **34**, 189 (2008).
[58] E. Kolbe, K. Langanke, and G. M. Fuller, Phys. Rev. Lett. **92**, 111101 (2004).
[59] P. Magierski and P. H. Heenen, Phys. Rev. C **65**, 045804 (2002).
[60] W. G. Newton and J. R. Stone, Phys. Rev. C **79**, 055801 (2009).
[61] F. J. Viñas and G. Madurga, Nucl. Phys. A **240**, 109 (1975).
[62] J. Błocki, J. Randrup, W. J. Swiatecki, and C. F. Tsang, Ann. Phys. (NY) **105**, 427 (1977).
[63] B. Grammaticos, Ann. Phys. (NY) **139**, 1 (1982).
[64] W. D. Myers and W. J. Swiatecki, Phys. Rev. C **57**, 3020 (1998).
[65] B. Liu, V. Greco, V. Baran, M. Colonna, and M. Di Toro, Phys. Rev. C **65**, 045201 (2002).
[66] A. Akmal, V. R. Pandharipande, and D. G. Ravenhall, Phys. Rev. C **58**, 1804 (1998).
[67] F. Sammarruca, Int. J. Mod. Phys. E **19**, 1743 (2010).
[68] E. N. E. van Dalen and H. Müther, Phys. Rev. C **82**, 014319 (2010).
[69] W. D. Myers and W. J. Swiatecki, Nucl. Phys. **81**, 1 (1966).
[70] W. D. Myers and W. J. Swiatecki, Annu. Rev. Nucl. Part. Sci. **32**, 309 (1982).
[71] W. D. Myers and W. J. Swiatecki, Phys. Rev. C **58**, 3368 (1998).
[72] K. Pomorski and J. Dudek, Phys. Rev. C **67**, 044316 (2003).
[73] P. Salamon, A. T. Kruppa, and T. Vertse, Phys. Rev. C **81**, 064322 (2010).
[74] J. Rikovska Stone, J. C. Miller, R. Koncewicz, P. D. Stevenson, and M. R. Strayer, Phys. Rev. C **68**, 034324 (2003).
[75] M. Farine, Z. Phys. A **321**, 265 (1985).
[76] M. Centelles, M. D. Estal, and X. Viñas, Nucl. Phys. A **635**, 193 (1998).
[77] M. Kleban, B. Nerlo-Pomorska, J.-F. Berger, J. Decharge, M. Girod, and S. Hilaire, Phys. Rev. C **65**, 024309 (2002).
[78] J.-F. Berger, M. Girod, and D. Gogny, Comput. Phys. Comm. **63**, 365 (1991).
[79] B. Nerlo-Pomorska and K. Mazurek, Phys. Rev. C **66**, 064305 (2002).
[80] G. A. Lalazissis, J. König, and P. Ring, Phys. Rev. C **55**, 540 (1997).
[81] A. T. Kruppa, M. Bender, W. Nazarewicz, P.-G. Reinhard, T. Vertse, and S. Ćwiok, Phys. Rev. C **61**, 034313 (2000).
[82] T. Vertse, A. T. Kruppa, and W. Nazarewicz, Phys. Rev. C **61**, 064317 (2000).
[83] S. Ćwiok, W. Dudek, P. Kaszyński, and W. Nazarewicz, Eur. Phys. J. A **23**, 387 (2005).
[84] J. Bartel, P. Quentin, M. Brack, C. Guet, and H. B. Håkansson, Nucl. Phys. A **386**, 79 (1982).
[85] J. Dobaczewski, H. Flocard, and J. Treiner, Nucl. Phys. A **422**, 103 (1984).
[86] M. Samyn, S. Goriely, P.-H. Heenen, J. M. Pearson, and F. Tondeur, Nucl. Phys. A **700**, 142 (2002).
[87] S. Goriely, M. Samyn, M. Bender, and J. M. Pearson, Phys. Rev. C **68**, 054325 (2003).
[88] E. Chabanat, P. Bonche, P. Haensel, J. Meyer, and R. Schaeffer, Nucl. Phys. A **635**, 231 (1998).
[89] P.-G. Reinhard and H. Flocard, Nucl. Phys. A **584**, 467 (1995).
[90] P.-G. Reinhard, D. J. Dean, W. Nazarewicz, J. Dobaczewski, J. A. Maruhn, and M. R. Strayer, Phys. Rev. C **60**, 014316 (1999).
[91] P.-G. Reinhard, M. Rufa, J. Maruhn, W. Greiner, and J. Friedrich, Z. Phys. A **323**, 13 (1986).

[92] M. Rufa, P.-G. Reinhard, J. A. Maruhn, W. Greiner, and M. R. Strayer, Phys. Rev. C **38**, 390 (1988).
[93] M. Bender, K. Rutz, P.-G. Reinhard, J. A. Maruhn, and W. Greiner, Phys. Rev. C **60**, 034304 (1999).
[94] R. W. Hasse and W. D. Myers, *Geometrical Relationships of Macroscopic Nuclear Physics* (Springer, Berlin, 1988).
[95] B. Singh, R. Zywina, and R. B. Firestone, Nucl. Data Sheets **97**, 241 (2002).
[96] E. A. Henry *et al.*, Z. Phys. A **338**, 469 (1991); Phys. Rev. C **49**, 2849 (1994).
[97] R. G. Henry *et al.*, Phys. Rev. Lett. **73**, 777 (1994).
[98] A. Lopez-Martens *et al.*, Phys. Rev. Lett. **77**, 1707 (1996).
[99] K. Hauschild *et al.*, Phys. Rev. C **55**, 2819 (1997).
[100] A. N. Wilson, G. D. Dracoulis, A. P. Byrne, P. M. Davidson, G. J. Lane, R. M. Clark, P. Fallon, A. Görgen, A. O. Macchiavelli, and D. Ward, Phys. Rev. Lett. **90**, 142501 (2003).
[101] A. N. Wilson *et al.*, Phys. Rev. Lett. **95**, 182501 (2005).
[102] M. V. Stoitsov, J. Dobaczewski, W. Nazarewicz, and P. Ring, Comput. Phys. Commun. **167**, 43 (2005).
[103] J. Dobaczewski and J. Dudek, Phys. Rev. C **52**, 1827 (1995).
[104] J. Dobaczewski and J. Dudek, Comput. Phys. Commun. **102**, 166 (1997); **102**, 183 (1997).
[105] J. Dobaczewski and P. Olbratowski, Comput. Phys. Commun. **158**, 158 (2004).
[106] J. Dobaczewski and P. Olbratowski, Comput. Phys. Commun. **167**, 214 (2005).
[107] J. Dobaczewski *et al.*, Comput. Phys. Commun. **180**, 2361 (2009).
[108] J. Dobaczewski, W. Nazarewicz, and T. R. Werner, Phys. Scr. **T56**, 15 (1995).
[109] J. Dobaczewski, W. Nazarewicz, and M. V. Stoitsov, Eur. Phys. J. A **15**, 21 (2002).
[110] A. Staszczak, M. Stoitsov, A. Baran, and W. Nazarewicz, Eur. Phys. J. A **46**, 85 (2010).
[111] J. Decharge and D. Gogny, Phys. Rev. C **21**, 1568 (1980).
[112] W. Younes and D. Gogny, Phys. Rev. C **80**, 054313 (2009).
[113] W. Nazarewicz, Phys. Lett. B **305**, 195 (1993).
[114] M. Bender, K. Rutz, P.-G. Reinhard, and J. A. Maruhn, Eur. Phys. J. A **7**, 467 (2000).
[115] S. Takahara, N. Takima, and N. Onishi, Nucl. Phys. A **642**, 461 (1998).
[116] P. H. Heenen, J. Dobaczewski, W. Nazarewicz, P. Bonche, and T. L. Khoo, Phys. Rev. C **57**, 1719 (1998).
[117] A. K. Dutta and M. Kohno, Nucl. Phys. A **349**, 455 (1980).
[118] F. Tondeur, Nucl. Phys. A **442**, 460 (1985).
[119] T. Bürvenich, M. Bender, J. A. Maruhn, and P.-G. Reinhard, Phys. Rev. C **69**, 014307 (2004).
[120] C. Guet, H.-B. Håkansson, and M. Brack, Phys. Lett. B **97**, 7 (1980).
[121] J.-F. Berger, M. Girod, and D. Gogny, Nucl. Phys. A **428**, 23c (1984).
[122] S. Goriely, M. Samyn, and J. M. Pearson, Phys. Rev. C **75**, 064312 (2007).
[123] M. Bender, P.-H. Heenen, and P. Bonche, Phys. Rev. C **70**, 054304 (2004).
[124] P. Bonche, J. Dobaczewski, H. Flocard, P.-H. Heenen, S. J. Krieger, and M. S. Weiss, Nucl. Phys. A **519**, 509 (1990).
[125] M. Bender, P. Bonche, T. Duguet, and P.-H. Heenen, Phys. Rev. C **69**, 064303 (2004).
[126] L. Bennour, P-H. Heenen, P. Bonche, J. Dobaczewski, and H. Flocard, Phys. Rev. C **40**, 2834 (1989).

[127] B. A. Brown, Phys. Rev. C **58**, 220 (1998).

[128] F. L. Braghin, D. Vautherin, and A. Abada, Phys. Rev. C **52**, 2504 (1995).

[129] F. Tondeur, S. Goriely, J. M. Pearson, and M. Onsi, Phys. Rev. C **62**, 024308 (2000).

[130] J. C. Pei, M. V. Stoitsov, G. I. Fann, W. Nazarewicz, N. Schunck, and F. R. Xu, Phys. Rev. C **78**, 064306 (2008).

[131] M. Horoi, A. Volya, and V. Zelevinsky, Phys. Rev. Lett. **82**, 2064 (1999).

[132] P. Maris, J. P. Vary, and A. M. Shirokov, Phys. Rev. C **79**, 014308 (2009).

[133] G. Hagen, D. J. Dean, M. Hjorth-Jensen, T. Papenbrock, and A. Schwenk, Phys. Rev. C **76**, 044305 (2007).

[134] S. Kvaal, Phys. Rev. B **80**, 045321 (2009).

[135] G. Audi, A. H. Wapstra, and C. Thibault, Nucl. Phys. A **729**, 337 (2003).

[136] K. Pomorski, Phys. Rev. C **70**, 044306 (2004).

[137] J. Dudek, W. Nazarewicz, and P. Rozmej, J. Phys. G **6**, 1521 (1980).

[138] B. Nerlo-Pomorska, Z. Phys. A **293**, 9 (1979).

[139] R. Bengtsson, J. Dudek, W. Nazarewicz, and P. Olanders, Phys. Scr. **39**, 196 (1989).

[140] S. Mizutori, J. Dobaczewski, G. A. Lalazissis, W. Nazarewicz, and P.-G. Reinhard, Phys. Rev. C **61**, 044326 (2000).

[141] L. Bonneau, P. Quentin, and D. Samsoen, Eur. Phys. J. A **21**, 391 (2004).

[142] A. Staszczak, A. Baran, J. Dobaczewski, and W. Nazarewicz, Phys. Rev. C **80**, 014309 (2009).

[143] G. I. Bell, Phys. Rev. **158**, 1127 (1967).

[144] J. Denschlag, in *Handbook of Nuclear Chemistry*, edited by A. Vértes, S. Nagy, Z. Klencsár, R. G. Lovas, and F. Rösch (Springer, Berlin, 2003).

[145] L. G. Moretto, Nucl. Phys. A **182**, 641 (1972).

[146] S. J. Lee and A. Z. Mekjian, Phys. Rev. C **82**, 064319 (2010).

[147] [http://unedf.org].

[148] G. F. Bertsch, D. J. Dean, and W. Nazarewicz, SciDAC Rev. **6**, 42 (2007) [http://www.scidacreview.org/0704/html/unedf.html].